Brain Stimulation 12 (2019) 877–892

Contents lists available at ScienceDirect

Brain Stimulation

journal homepage: http://www.journals.elsevier.com/brain-stimulation

Consistent linear and non-linear responses to invasive electrical brain stimulation across individuals and primate species with implanted electrodes

Ishita Basu [a, b, 2], Madeline M. Robertson [a, 2], Britni Crocker [c], Noam Peled [d], Kara Farnes [a, c], Deborah I. Vallejo-Lopez [c], Helen Deng [a, d], Matthew Thombs [a, 3], Clarissa Martinez-Rubio [a], Jennifer J. Cheng [a], Eric McDonald [a], Darin D. Dougherty [b], Emad N. Eskandar [a, 3, 1], Alik S. Widge [b, e, 4, 1], Angelique C. Paulk [a, c, *, 1], Sydney S. Cash [c, 1]

[a] Nayef Al-Rodhan Laboratories, Department of Neurosurgery, Massachusetts General Hospital and Harvard Medical School, Boston, MA 02114, USA
[b] Department of Psychiatry, Massachusetts General Hospital and Harvard Medical School, Charlestown, MA, 02129, USA
[c] Department of Neurology, Massachusetts General Hospital, Boston, MA 02114, USA
[d] Department of Radiology, MGH/HST Martinos Center for Biomedical Imaging, Charlestown, MA, 02129, USA
[e] Picower Institute for Learning & Memory, Massachusetts Institute of Technology, Cambridge, MA 02124, USA

ARTICLE INFO

Article history:
Received 31 July 2018
Received in revised form
5 March 2019
Accepted 6 March 2019
Available online 11 March 2019

Keywords:
Cingulate cortex
Frequency
Current
Local field potential
Neuromodulation
Intracranial

ABSTRACT

Background: Electrical neuromodulation via implanted electrodes is used in treating numerous neurological disorders, yet our knowledge of how different brain regions respond to varying stimulation parameters is sparse.
Objective/Hypothesis: We hypothesized that the neural response to electrical stimulation is both region-specific and non-linearly related to amplitude and frequency.
Methods: We examined evoked neural responses following 400 ms trains of 10–400 Hz electrical stimulation ranging from 0.1 to 10 mA. We stimulated electrodes implanted in cingulate cortex (dorsal anterior cingulate and rostral anterior cingulate) and subcortical regions (nucleus accumbens, amygdala) of non-human primates (NHP, N = 4) and patients with intractable epilepsy (N = 15) being monitored via intracranial electrodes. Recordings were performed in prefrontal, subcortical, and temporal lobe locations.
Results: In subcortical regions as well as dorsal and rostral anterior cingulate cortex, response waveforms depended non-linearly on frequency (Pearson's linear correlation $r < 0.39$), but linearly on current ($r > 0.58$). These relationships between location, and input-output characteristics were similar in homologous brain regions with average Pearson's linear correlation values $r > 0.75$ between species and linear correlation values between participants $r > 0.75$ across frequency and current values per brain region. Evoked waveforms could be described by three main principal components (PCs) which allowed us to successfully predict response waveforms across individuals and across frequencies using PC strengths as functions of current and frequency using brain region specific regression models.
Conclusions: These results provide a framework for creation of an atlas of input-output relationships which could be used in the principled selection of stimulation parameters per brain region.

Abbreviations: NHP, Non-human primate; dACC, Dorsal anterior cingulate cortex; rACC, Rostral anterior cingulate cortex; NAcc, Nucleus accumbens; ERP, event-related potential; LFP, local field potential; PCA, principal components analysis; ELA, electrode labeling algorithm; CxF, current * frequency value.

* Corresponding author. Nayef Al-Rodhan Laboratories, Department of Neurosurgery, Massachusetts General Hospital and Harvard Medical School, Boston, MA 02114, USA.
E-mail address: apaulk@mgh.harvard.edu (A.C. Paulk).

[1] Authors are considered co-senior authors on the manuscript.
[2] These authors contributed equally to this work.
[3] Present address: Department of Neurosurgery, Albert Einstein College of Medicine, Montefiore Medical Center, Bronx, NY 10467, USA.
[4] Present address: Department of Psychiatry, University of Minnesota, Minneapolis, MN 55455, USA

https://doi.org/10.1016/j.brs.2019.03.007

Introduction

Pulsatile electrical stimulation of the brain parenchyma via implanted intracranial electrodes is employed clinically to treat movement, psychiatric, and seizure disorders [1–6], but the mechanisms by which stimulation modulates neural activity are highly debated [6–10]. Different frequencies affect different diseases [6,8]: high frequency stimulation (>100 Hz) treats Parkinson's disease [10–12], while a lower frequency range (~10 Hz) may interrupt seizures [11,13]. Little is known about the effects of different frequencies on neural circuitry or why specific frequencies are less effective in certain diseases [3,6,8,10]. Theoretical approaches have focused on modeling the spread of current from implanted electrodes [14,15], and empirical work on the general physiology of invasive neurostimulation has focused heavily on avoiding tissue damage or over-excitation [16,17]. There is also a large body of work exploring the physics of non-invasive stimulation, much of it focused on modeling how patient anatomy influences magnetic and electrical field propagation into cortex [18–23]. There have, however, been few systematic explorations of the large stimulation parameter space commonly used in invasive applications [11,12,24–28]. Consequently, little is known about the input-output relationships between stimulation parameters and neuronal activity. More specifically, a major question is whether the neural response at the level of the population is directly proportional to the level of injected current or the frequency of the stimulation, or whether this input-output relationship to stimulation parameters is non-linear (although potentially still monotonic). A second question is how consistent this population neural response is between individuals and across species.

We systematically evaluated this input-output relationship in multiple brain regions. We performed multi-trial tests of stimulation trains with varying frequency and amplitude in non-human primates (NHPs) and tested a subregion of the frequency by current landscape in humans. We mapped responses in dorsal and rostral anterior cingulate cortex (dACC and rACC, respectively), amygdala, and nucleus accumbens (NAcc). These regions have long been therapeutic targets for invasive neuromodulation [4,5,29–35]. We used the evoked potential (ERP) as the primary readout [36–39], which has been suggested to predict the clinical response to therapeutic invasive stimulation [40–42]. The cortical targets responded linearly to changes in stimulation amplitude and non-linearly to changes in frequency. Subcortical targets, including the amygdala in humans and NAcc in NHPs, showed a linear input-output relationship. These results demonstrate the feasibility of an atlas of neural responses, which should enable more rational therapeutic planning.

Materials and Methods

Human participants

We recorded from 15 participants (mean age = 37.42, ranging from 19 to 56; 10 females; Table A 1) with intractable epilepsy undergoing invasive monitoring for surgical treatment of seizures. Participants were implanted with multi-lead depth electrodes (a.k.a sEEG) to locate epileptogenic tissue in relation to essential cortex. Depth electrodes (Ad-tech Medical, Racine WI, USA, or PMT, Chanhassen, MN, USA) with diameters of 0.8–1.0 mm and consisting of 8–16 platinum/iridium-contacts 1–2.4 mm long were stereotactically placed in locations deemed necessary for seizure localization by a multidisciplinary clinical team. Following implant, the preoperative T1-weighted MRI was aligned with a post-operative CT using volumetric image co-registration procedures and FreeSurfer scripts ([43,44]; http://surfer.nmr.mgh.harvard.edu). Electrode coordinates were manually determined from the CT in the patients' native space [45] and mapped using an electrode labeling algorithm (ELA [46]) that registered each contact to a standardized cortical map [47]. To visualize all the electrodes in the same space (a single brain representation), we performed a nonlinear transformation of the locations of the electrodes from each patient's native space to a template MRI (27 [48]) using FreeSurfer tools ([49]).

Electrode contacts in rACC, dACC, and amygdala that did not show epileptiform activity were selected for stimulation experiments. Participants received their normal antiepileptic medications to minimize the risk of seizure during stimulation.

Ethics statement

All patients voluntarily participated after fully informed consent according to NIH and Army Human Research Protection Office (HRPO) guidelines as monitored by the Massachusetts General Hospital (MGH) Institutional Review Board (IRB). Participants were informed that participation in the experiment would not alter their clinical treatment in any way, and that they could withdraw at any time without jeopardizing their clinical care.

Non-human primates

Experimental procedures were carried out according to the Guide to the Care and Use of Laboratory Animals provided by the Public Health Service. All efforts were made to minimize discomfort, and the Institutional Animal Care and Use Committee at the Massachusetts General Hospital monitored care and approved all procedures. Intracranial recordings were acquired from four adult male rhesus macaques (*Macaca mulatta*; 10–14 years old at date of implant). Each NHP was implanted with a recording chamber that allowed access to right hemisphere targets mirroring the regions studied in human participants. Trajectories for electrode implant were calculated by mapping target regions to a post-chamber magnetic resonance imaging (MRI) with fiducial markers and MANGO software (San Antonio, TX). Implantation included the dorso-lateral pre-frontal cortex (dlPFC), dACC, rACC, and NAcc (Supplementary Fig. 1, Table A 2). Following implant, electrode locations were confirmed through co-registration of the subject's preoperative MRI and postoperative CT using MANGO. Reconstructions of brain regions used custom MATLAB programs and MANGO software to visualize electrode locations relative to three atlases [50–54]. Finally, the volume reconstructions and electrode locations were visualized in Blender (https://www.blender.org/). Animals were implanted for a period of one month (NHP 1) to a full year (NHP 2) and then were explanted to enable full recovery. No clear adverse behavioral effects were observed before or after electrode implant or explant.

Data acquisition

NHP extracellular recordings were digitized at 40 kHz using an OmniPlex system (Plexon, Dallas, TX, USA) and were filtered to capture the local field potential (LFP; filter: 0.5–500 Hz, online decimated to 1000 Hz). Recordings were referenced to the titanium head post.

Human recordings used a Blackrock system with a sampling rate of 2 kHz (Blackrock Microsystems, Salt Lake City, UT, USA). Depth recordings were referenced to an EEG electrode placed on skin (C2 vertebra or Cz).

Neural stimulation

Parallel stimulation experiments were carried out in humans and NHPs. Limited by the experimental time window and safety reasons, we were unable to explore as extensive a range of frequencies and currents in humans as in NHPs. Both human and NHP subjects had 1 stimulation session in a day. A typical NHP stimulation session consisted of 200–350 stimulation trials. Each trial delivered a 400 ms train (90 μs charge-balanced biphasic symmetrical pulses with an interphase interval of 53 μsec) with varying pulse frequencies (10–400 Hz) and amplitudes (0.2–10 mA). Each trial was separated by 5 s with randomized jitter up to ±1 s and the frequencies were randomized for a fixed current amplitude. Current injection and return paths used neighboring contacts, driven by a stimulus isolator (A-M Systems Model 3800 8 channel stimulator with Model 3820 Stimulation Isolation Unit, Sequim, WA) controlled via MATLAB. Five trials of each frequency/amplitude combination were delivered per session (Table A 3). Each trial's current and frequency were randomly selected. NHPs underwent stimulation while awake and resting in a Faraday cage that was actively monitored by an experimenter.

Human stimulation sessions used the same bipolar electrode configuration, pulse shape, and train duration as in NHPs. Stimulation delivered with a CereStim (Blackrock Microsystems, Salt Lake City, UT) ranged from 10 to 160 Hz and currents from 1 to 8 mA (Table A 3). In our stimulation location selection, we attempted to select cingulate sites which were similar between participants, particularly at the grey-white matter boundary in the cortex. For the amygdala, we selected sites which were well within the center of the amygdala. We started at the lowest current level while a trained electroencephalographer examined ongoing recordings for epileptiform activity and asked participants if they experienced any sensations. If there was neither epileptiform activity nor subjective effects, we continued to the next current level until we reached either 6 mA or 8 mA. Trial frequencies were randomized within an amplitude level (Table A 3). The participants were aware that they were being stimulated but were blind to the stimulation timing and parameters.

Data analysis

Data analysis was performed using MATLAB. Data were decimated to 1000 Hz and demeaned. Line noise (60, 120, 180 Hz) was removed by subtracting band-passed signals from the raw signal. Recordings were bipolar re-referenced by subtracting the activity of adjacent electrode contact pairs. Channels with excessive line noise or without clear neural signal were removed from the analysis. For human data, based on both clinical reports and visual inspection, electrodes surrounding the epileptic focus and/or exhibiting abnormal activity were excluded from analysis. The ERP was analyzed by extracting epochs from 600 ms before stimulation onset to 2500 ms after offset. The mean voltage of a baseline segment, 500 ms preceding stimulation, was subtracted from each data point. We calculated several ERP metrics: normalized peak amplitude, time to peak, area under the curve of absolute voltages, voltage standard deviation, normalized minimum voltage (valley amplitude), and time to minimum. Peaks and valleys were automatically detected as the maximum and minimum ERP voltages in an 800 ms post-stimulation window. Voltages were normalized by dividing by the standard deviation of the baseline data segment. Area under the curve was the sum of the absolute values of data for 800 ms after stimulation offset. We only analyzed peak and valley amplitudes/times when the post-stimulation voltage deflection was at least 3 standard deviations from the average voltage of a 500 ms pre-stimulation baseline period. Time to peak/minimum was determined as the time difference between the end of stimulation train and the peak/valley amplitude of the following ERP. Pearson's linear correlation was then used to correlate amplitude ERP metrics (normalized peak amplitude, area under the curve of absolute voltages, voltage standard deviation, normalized minimum voltage) with frequency and current separately and then averaged per individual and then across individuals.

Data recorded across all implanted electrode pairs were subdivided into local responses and network responses to separate the waveform characteristics nearest to the stimulation from the spread throughout the brain. Local responses are the ERPs from a single pair of electrodes adjacent to the stimulating electrode pair; the global responses were from all other channel pairs across the brain spanning amygdala, hippocampus, cingulate, pre-frontal, orbito-frontal and temporal cortices (Supplementary Figures 1, 2). For network response calculations, we averaged the absolute z-scored voltages for the 1 s following stimulation for channels across the brain and per recorded brain region per individual, followed by averaging these values across individuals. Due to narrower brain region coverage, we did not perform the per-brain region analysis for NHPs.

Principal component analysis was carried out across post-stimulus ERPs. Using the MATLAB 'princomp' function and treating time as the variable and the individual per-trial waveforms across brain regions and subjects as observations, we calculated the first 20 principal components (PCs) for the normalized voltages and found that the first two PCs explained >80% of the variance. We then examined how different currents and frequencies varied the ERP waveform scores for principal components 1 (PC1), 2 (PC2), and 3 (PC3) by projecting each mean ERP through each PC basis. Finally, we mapped the sites which had the largest absolute PC scores (absolute values greater than 100) to a common brain map.

Analysis of variability between stimulation sites per brain region

To examine consistency across individuals, we performed two types of analyses. In one case, we performed a Pearson's linear correlation calculation of the z-scored waveforms per current and frequency step between each pair of individual NHP or human ERP data sets and pairwise between each individual in the human data set, averaging across all combinations per current and frequency. In the second measure, we performed a two-dimensional cross correlation between individuals for the ERP metric and PC current x frequency (CxF) maps through an iterative sampling method for the cingulate stimulation sites. We averaged the current x frequency map across six stimulation sites randomly sampled from the entire data set, then performed cross correlations with each of the remaining four individual current x frequency maps (in the dACC) and remaining five maps (in the rACC) to get an r value per remaining current x frequency map. We repeated this random sampling process 100 times, for both ERP metrics and PC scores, to estimate a confidence interval for the cross-correlation.

Linear model fit and ERP prediction using PC scores

To demonstrate that stimulation responses could be predicted from prior subjects' data, we fit linear regression models (MATLAB 'fitlm') to brain-region-specific PC scores as functions of frequency and current. The general form of this model is:

$$Y = a_0 + a_1 * x_f + a_2 * x_c + a_3 * x_f * x_c + a_4 * x_f^2 + a_5 * x_c^2$$

Where Y is the PC score, x_f is the stimulation frequency and x_c is the stimulation current.

We created 3 models: one a linear model in frequency and current ($Y = a_0 + a_1 * x_f + a_2 * x_c$), the second with an interaction term added ($Y = a_0 + a_1 * x_f + a_2 * x_c + a_3 * x_f * x_c$) and, finally, the full model containing quadratic terms. For any given region we selected the model which was significantly different from a constant model ($Y = a_0$) and had the highest R^2. If none of these models was significant, we concluded that the particular PC score did not have a linear or quadratic functional relationship with stimulation current and frequency.

We then tested the predictive power of the models in two ways: 1) For each dACC and rACC dataset, model parameters were based on data from all but one participant for a leave one out comparison; 2) A model was trained using stimulation frequencies of 10, 40, 100, and 160 Hz across all datasets. We then predicted the PC scores and reconstructed z-scored voltage ERPs for the remaining frequencies.

Statistical analysis

All statistical comparisons used non-parametric measures except the two-way ANOVA, which was only done to examine possible interaction effects of current and frequency on the ERP metrics. Otherwise, we tested non-equivalence of multiple medians with a Kruskal–Wallis test followed by the *post hoc* Tukey-Kramer method to determine statistically separable groups. We used the Wilcoxon rank sum test (two-sided) for comparisons between two medians. For the current x frequency maps, we performed the Wilcoxon rank sum test of each entry in the matrix against values at current = 2 mA and frequency = 10 Hz. We additionally used the Wilcoxon signed rank test (two-sided) for determining if a distribution's median, such as a distribution of correlation values or PC scores, was significantly different from zero. We corrected for multiple comparisons by adjusting the target p-value (0.05) with a Bonferroni correction for the number of comparisons being done for each analysis. For data points across the current multiplied by frequency (CxF) x-axis values, we further applied a false discovery rate (FDR) correction to the p-value following Kruskal-Wallis comparisons between data points since each data point contained multiple trials per frequency and current combination per individual. We performed a two-way ANOVA to examine the effect of the independent variables (current and frequency stimulation parameters) on the dependent variables, namely the ERP metrics responses in the human and NHP data set.

Results

Neural responses to trains of stimulation show 'hot spots' with changing current and frequency

We recorded ERPs from stimulation in 4 NHPs and 15 humans (Fig. 1A–C; Supplementary Figures 1-2; Table A 1-A 3). ERPs in local channels after dACC stimulation were highly consistent between individual NHPs and humans (Fig. 1D–E) and showed a biphasic response to low frequency stimulation. With increasing frequency, responses became monophasic, with a delayed time to peak at the highest frequencies. Similar patterns were found with local rACC stimulation (Fig. 1F, Supplementary Fig. 3). Subcortical stimulation was more variable (Fig. 1G, Supplementary Fig. 3). To quantify this response, we measured ERP features: 1) amplitude metrics (normalized peak amplitude, area under the curve of absolute voltages, voltage standard deviation, normalized minimum voltage) and 2) timing metrics (time to peak, time to valley; Fig. 2A).

To determine the effects of current and frequency on these local ERP metrics, we performed a two-way ANOVA. Frequency had significant effects in 3/6 timing metrics, versus significant effects in 4/12 amplitude metrics across stimulated brain regions. On the other hand, current had significant effects on 11/12 ERP amplitude metrics versus no significant effect on the timing metrics (Table A 4). Interestingly, interactions between frequency and current were not significant, except for one rACC measure. This suggests that the effects of frequency and current on the ERP waveform are independent (Table A 4).

As evident in the individual response, current is a major driver of the ERP simply because, to get a neural response, we must reach a threshold. Yet, above a certain amplitude, frequency begins to play a role, particularly in the waveform timing (Table A 4). At fixed, sufficient current, ERPs exhibited a non-linear relationship with frequency as exemplified by a sigmoidal curve on the level of the individual (Fig. 2B; Supplementary Fig. 4-5). These trends are better reflected as a matrix of ERP metrics based on current x frequency which showed separable 'hot spots' (Fig. 2C and D; Supplementary Fig. 6). For dACC stimulation, peak amplitude was highest between 80 and 100 Hz with a plateau or even dip in the 130–160 Hz range. At high stimulation amplitudes, increasing frequency decreased ERP peak amplitude, which was not as obvious a trend for increasing current (Fig. 2B and C; Supplementary Fig. 6). This decrease in amplitude is especially obvious in NHP experiments in which stimulation frequency was increased to 400 Hz (Figs. 1D and 2C). These trends resulted in a lower linear correlation between ERP amplitude metrics and frequency across individuals compared to the correlation between current and ERP amplitude metrics, particularly with rACC and amygdala stimulation (human data; Pearson's r values: dACC: 0.39 ± 0.402 (frequency) vs 0.58 ± 0.231 (current); rACC: 0.18 ± 0.427 (frequency) vs 0.62 ± 0.161 (current); amygdala: 0.14 ± 0.347 (frequency) vs 0.66 ± 0.214 (current), Fig. 2E). In addition, response timing also varied with frequency with the time to peak and time to valley shorter for middle frequencies, though the exact pattern varied with brain region. (Fig. 2D and F; Supplementary Fig. 6).

Since neural output could reflect the totality of energy delivered to the tissue [12], we examined the relationship between current x frequency and ERP metrics. Increasing CxF increased the ERP amplitude, time to peak, and time to valley across brain regions and species (Fig. 3A and B; Supplementary Fig. 7). Remarkably, ERP metrics changed in concert with frequency changes even with similar overall injected energy (Kruskal-Wallis multiple comparisons; FDR corrected; Note: each color-coded dot is 5 trials per condition and individual; Fig. 3A–B; Supplementary Fig. 7). When subdividing ERP peak amplitudes into low (10–40 Hz), mid (80–100 Hz), high 100–200 Hz), and highest (>200 Hz) frequency bins, there were significant differences in peak amplitudes between the frequency ranges, particularly in the NHP NAcc and human rACC, further illustrating the nonlinear effect of frequency on waveforms ($p < 0.0001$; Kruskal-Wallis test; Fig. 3C and D).

Principal components analysis can also be used to map ERPs in the current x frequency space

To reduce dimensionality and better predict responses to untested currents and frequencies, we used principal component analysis (PCA [55]). The first three PCs explained ~80% of the local response variation (Fig. 4A; variation explained per PC: human: PC1-64.6%; PC2-29.9%; PC3-3.4%; NHP: PC1-68.3%; PC2-19.5; PC3-7.3%). PC1 captured early, long duration positive voltages while PC2 mostly captured a late negative voltage deflection and PC3 was more variable (Fig. 4B). When averaging activation (PC scores) across recorded brain regions, we found mean absolute PC1 scores significantly differed from zero at both low and high stimulation frequencies and at low and mid currents across all stimulation

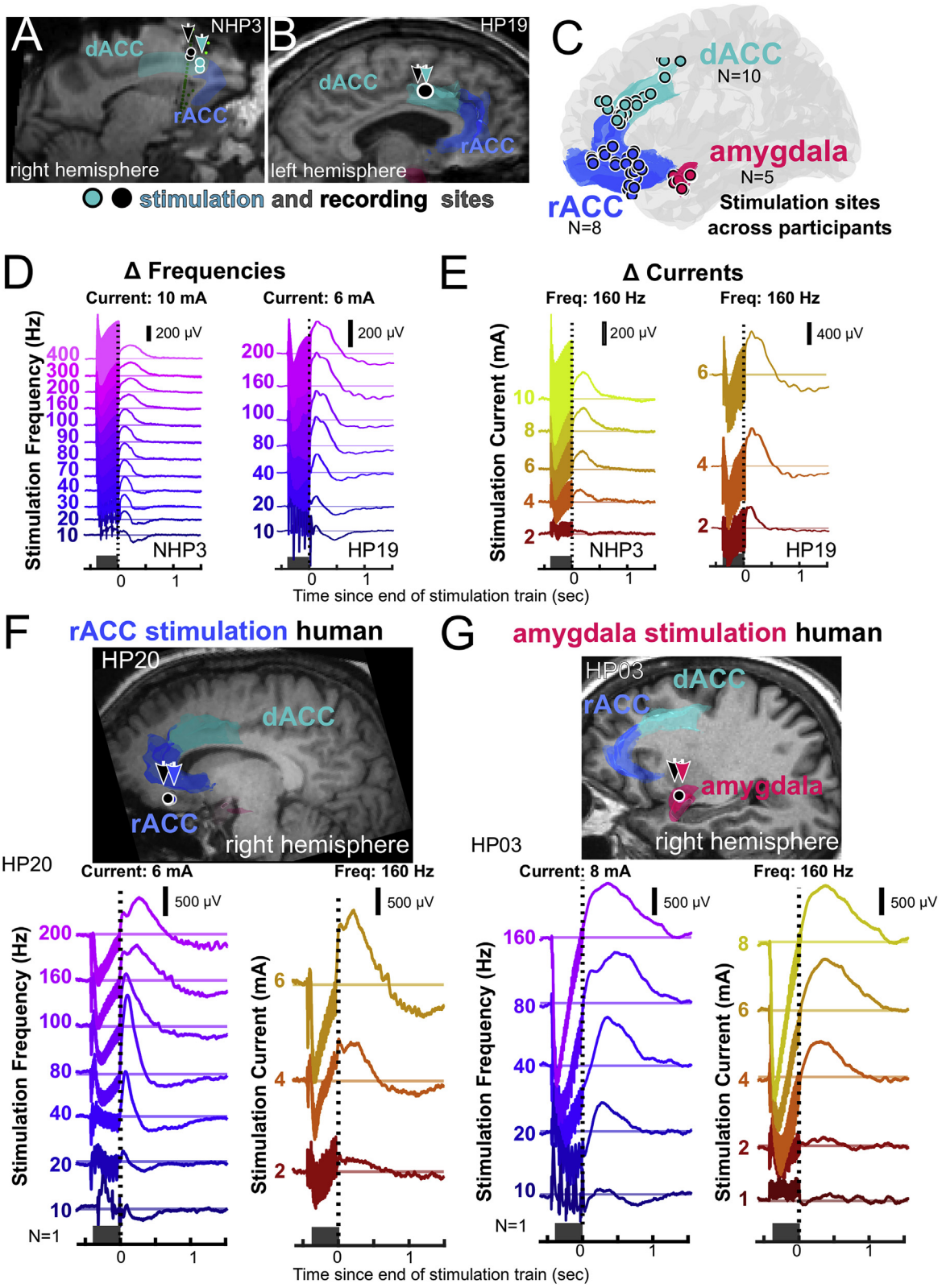

Fig. 1. Effects of current and frequency on the local event-related potential in multiple brain regions (ERP). A-B. dACC stimulation: MRI showing stimulating (teal circles) and recording (black circles) electrode locations in a non-human primate (NHP3) and (**B**) human participant (HP19). **C**. dACC (teal), rACC (blue), and amygdala (pink) stimulation locations for all participants mapped to a single standardized brain. **D**. dACC stimulation: Average neural responses to stimulation trains (grey bar) for different frequencies (color coded magenta to blue) at a stable current in NHP3 (left, at 10 mA) and HP19 (right, 6 mA). **E**. dACC stimulation: Local ERPs to stimulation trains for different currents (color coded red to yellow) at 160 Hz stimulation. **F**. rACC stimulation: MRI showing stimulating (blue circles) and recording (black circles) electrode locations in human participant (HP20, top). (bottom) Average neural responses to stimulation trains (grey bar) for different frequencies (color coded magenta to blue) at a stable current in HP20 (left, 6 mA) and for different currents (color coded red to yellow) at 160 Hz stimulation. **G**. amygdala stimulation: MRI showing stimulating (pink circles) and recording (black circles) electrode locations in human participant (HP03, top). (bottom) Average neural responses to stimulation trains (grey bar) for different frequencies (color coded magenta to blue) at a stable current in HP03 (left, 8 mA) and for different currents (color coded red to yellow) at 160 Hz stimulation. (For interpretation of the references to color in this figure legend, the reader is referred to the Web version of this article.)

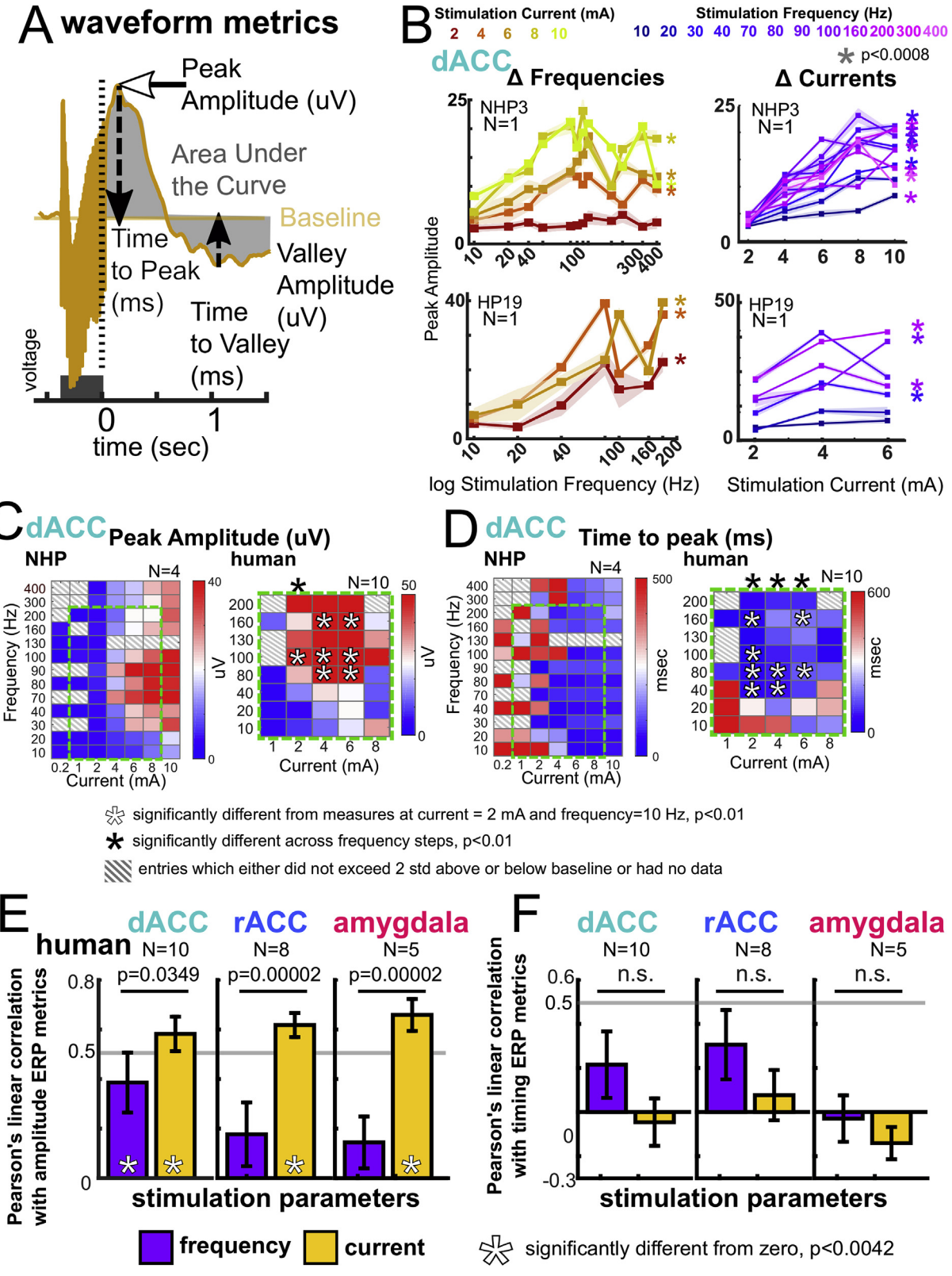

Fig. 2. Effects of current and frequency on the waveform of the local event-related potential (ERP). **A**. ERP metrics. **B**. Right: Peak amplitudes and standard error (mV) for the ERPs in NHP3 (top) and HP19 (bottom) for different frequencies, with each curve indicating a different current level. *- indicate values are significantly different across frequencies within a current level (left column) or significantly different across current values within a frequency level (right column), $p < 0.0008$, Kruskal-Wallis test. Left: Peak amplitudes and standard error (mV) for the ERPs in NHP3 (top) and HP19 (bottom) for different currents, with each curve indicating a different frequency level. **C-D**. Across-individual average local ERP peak amplitudes (mV) and time to peak (sec) with changes in frequency and current. Blue to white to red scales indicate increasing peak amplitudes. White *: significantly different from measures at current = 2 mA and frequency = 10 Hz, $p < 0.01$, Wilcoxon rank sum test. Black *: significantly different across frequency steps, $p < 0.01$, Kruskal-Wallis test. Green outline: Frequency and current space tested in both NHPs and human participants. **E-F**. Absolute Pearson's r correlations between ERP amplitude metrics (maximum peak, minimum peak, AUC, StDev) and frequency (**E**; purple bars) and current (yellow bars) and between ERP timing metrics (**F**; time to peak and time to valley); p-values denote significant differences, Wilcoxon rank sum test; white * indicate correlation values significantly different from zero, $p < 0.0042$; Wilcoxon signed rank test). (For interpretation of the references to color in this figure legend, the reader is referred to the Web version of this article.)

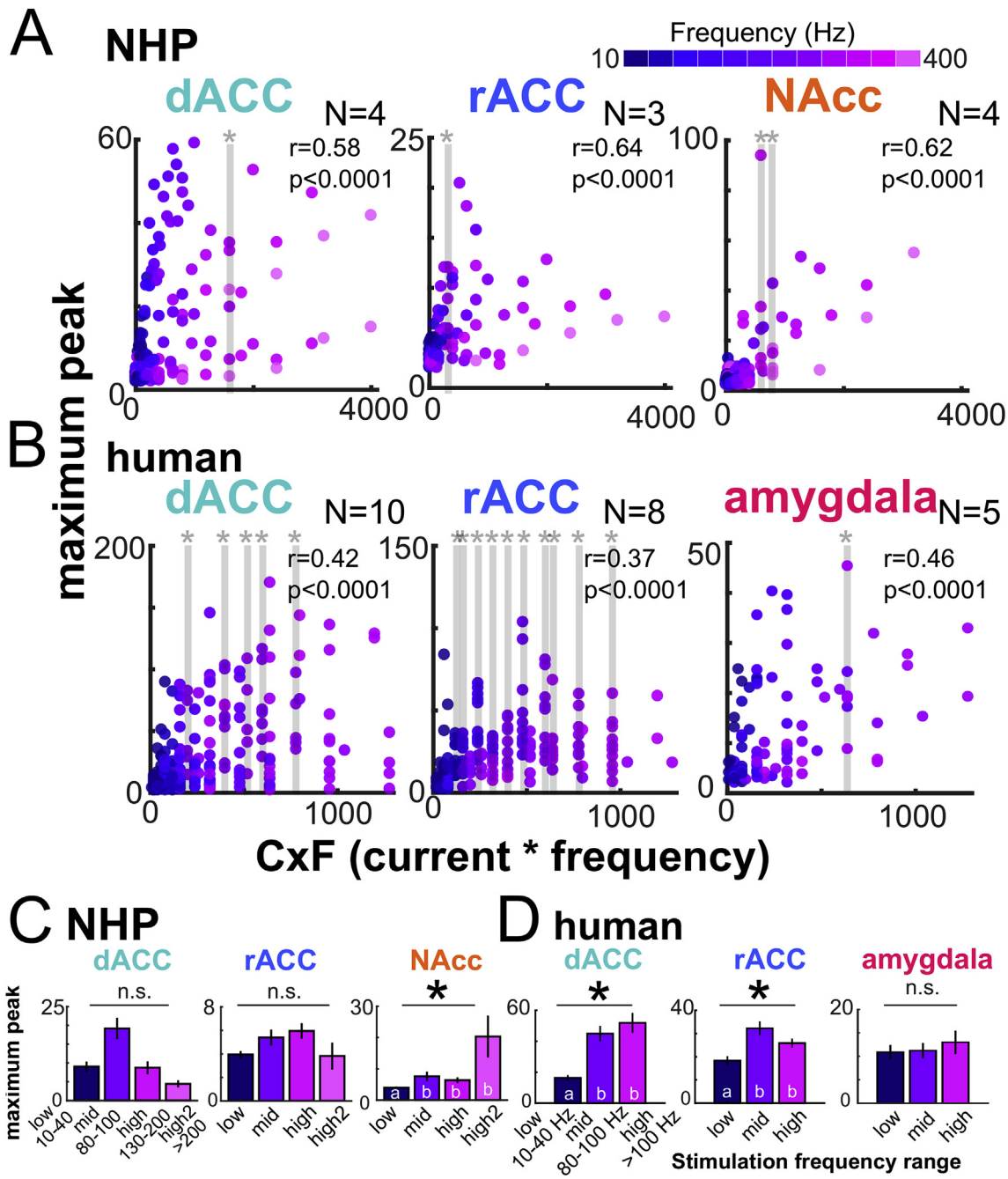

Fig. 3. Frequency alters the relationship between injected energy and local ERP responses. **A**. NHP and **B**. human participant ERP peaks, mapped against the current x frequency value. Each dot is an average peak per individual, color-coded by frequency (blue to pink). Vertical grey lines indicate significant differences between stimulation with the same current x frequency value but different frequencies. r values indicate Pearson's correlation values and p-values between CxF and mean maximum peak values. **C**. NHP and **D**. human average peak values subdivided into low (10–40 Hz), mid (80–100 Hz), high (130–200 Hz), and highest (high 2, >200 Hz) frequency ranges for different brain regions. *-$p < 0.0001$; significant differences between low, mid, and high frequency ranges, Kruskal-Wallis test. In **C-D**: a-b letters indicate separable groups, identified with a *post hoc* Tukey test. (For interpretation of the references to color in this figure legend, the reader is referred to the Web version of this article.)

regions (Fig. 4C). PC2 and PC3 had large mean absolute scores for amygdala stimulation but not for cingulate stimulation. The CxF metric (e.g. total energy) steadily increased PC1 but not PC2 or PC3 scores for dACC and amygdala stimulation (Fig. 4D). Indeed, both PC2 and PC3 scores decreased with higher CxF values with amygdala stimulation (Fig. 4D). Thus, PCA decomposition could separate the effects of total energy (CxF; PC1 spread) from current and frequency effects in the cingulate (which changed PC2 and PC3 spread), though this was not true with amygdala stimulation.

Similar to ERP peak amplitudes, PC1 scores were larger at high frequencies and currents in the dACC and rACC (human: $p < 0.01$; significantly different from 10 Hz/2 mA stimulation; Wilcoxon rank sum test; Fig. 5A and B). In contrast, PC2 had larger absolute scores representing a diagonal across low and middle frequencies and low to middle currents in the rACC and dACC (Fig. 3C and D). In other words, activation shifted from PC2 to PC1 waveforms as frequency/current increased along the diagonal from low frequency and

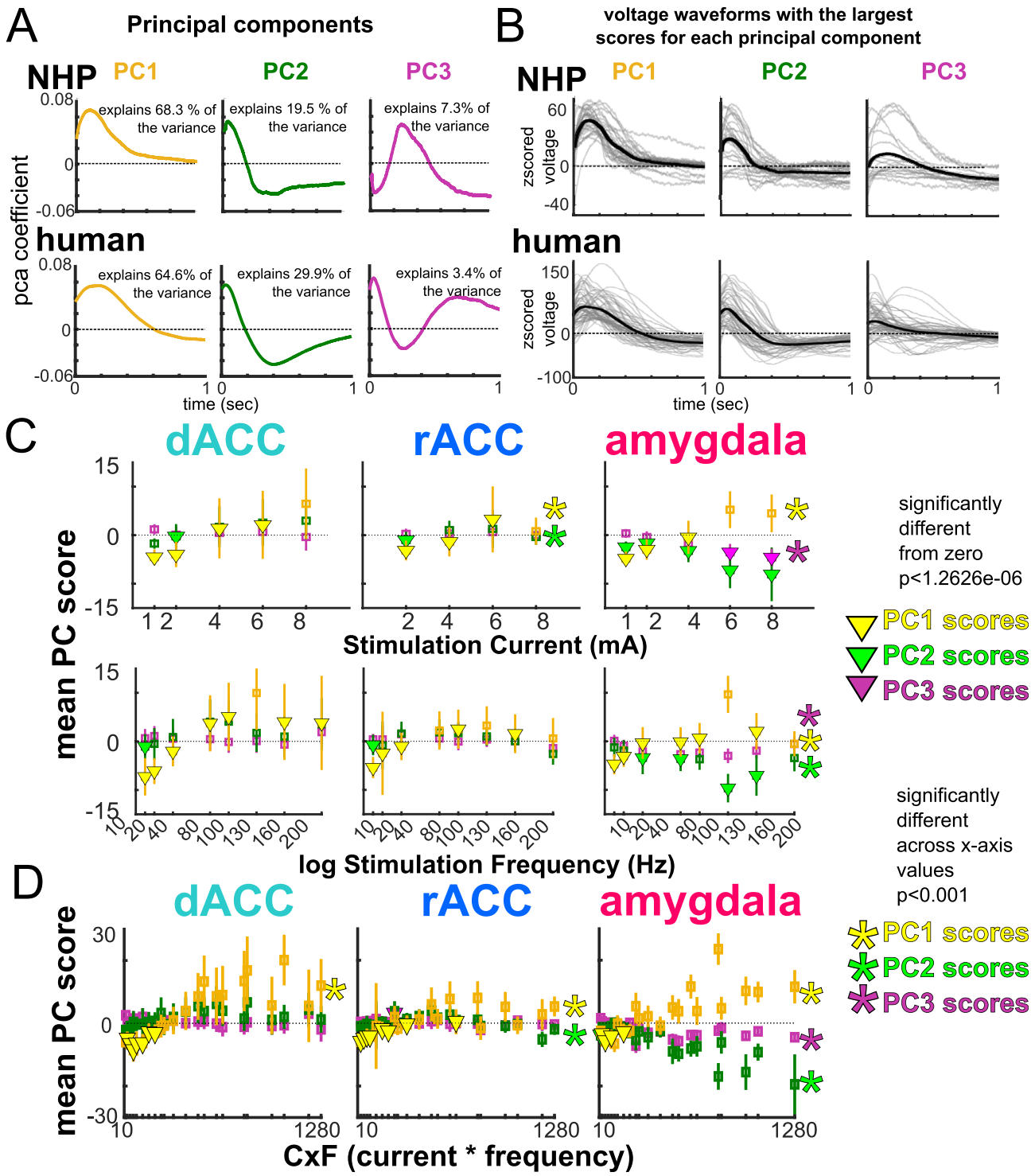

Fig. 4. Principal components analysis subdivides local ERP waveforms in both NHPs and human participants. **A**. PC coefficients calculated across waveforms for the local NHP ERP responses (top) and human participant ERP responses (bottom) for PC1 (yellow), and PC2 (green). **B**. Average z-scored local voltage waveforms in NHP (top) and human participant (bottom) with the largest PC1 scores (left column) and largest PC2 scores (right column). **C.** PC scores for principal component 1 (PC1, yellow), principal component 2 (PC2, green), and principal component 3 (PC3, maroon) across individuals and brain regions (global responses) mapped to changing currents (top plots) and changing frequencies (bottom) for dACC, rACC, and amygdala stimulation. **D**. Mean PC scores for current x frequency values for the different regions of stimulation (global responses). For **C** and **D**, yellow (PC1), green (PC2), and magenta (PC3) triangles indicate average scores significantly different from zero, $p < 1.2626e\text{-}06$, corrected for multiple comparisons. For **C-D**, * - indicates significant differences across x axis values (Kruskal-Wallis test) and error bars show standard deviation. (For interpretation of the references to color in this figure legend, the reader is referred to the Web version of this article.)

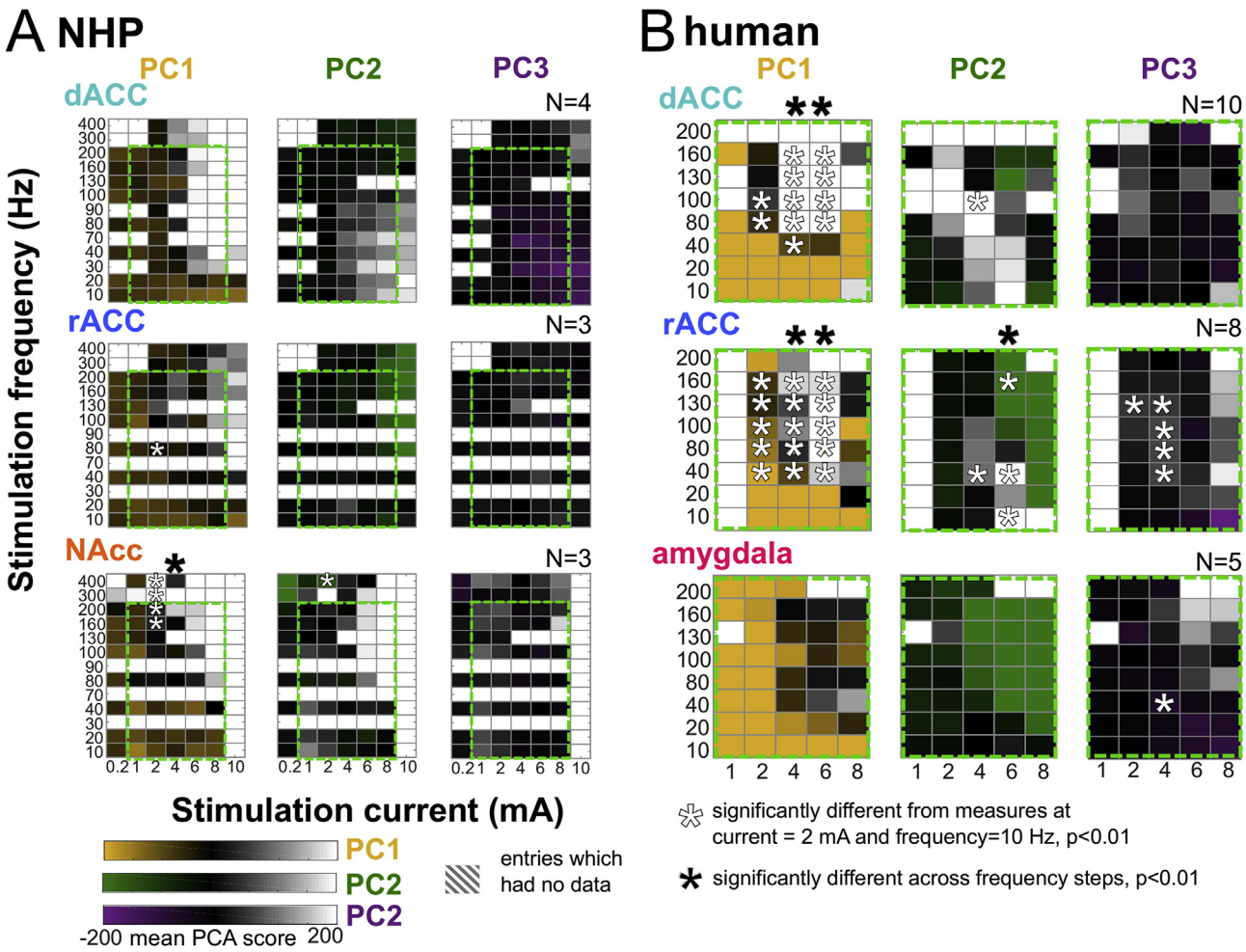

Fig. 5. Principal components map differentially across the current and frequency stimulation space. **A**. Mean PC1 (left), PC2 (middle), and PC3 (right) scores for local recording sites across frequencies and currents with dACC, rACC, and NAcc stimulation in NHPs. **B**. Mean PC1 (left), PC2 (middle), and PC3 (right) scores for local recording sites across frequencies and currents with dACC, rACC, and amygdala stimulation in human participants. Green outline boxes are described in Fig. 2. White *: significantly different from measures at current = 2 mA and frequency = 10 Hz, $p < 0.01$, Wilcoxon rank sum test. Black *: significantly different across frequency steps, $p < 0.01$, Kruskal-Wallis test. (For interpretation of the references to color in this figure legend, the reader is referred to the Web version of this article.)

current to high frequency and current while, once again, PC3 waveforms were more variable.

ERP waveform metric and PC score current x frequency maps are highly correlated across individuals

To determine if local responses were consistent, or correlated, between humans and NHPs and across individuals (Fig. 6A), we correlated the z-scored waveforms between each NHP and human participant and averaged the correlation values across comparisons per current and frequency step (Fig. 6B). We found large correlation values (>0.75) between the human and NHP data at high and middle frequencies (Fig. 6B). We then performed the same analysis using only the human data set and again found large correlation values across much of the matrix at middle and high current and frequency values (>0.75), though the correlation values were not significantly different from zero following multiple comparison corrections (Wilcoxon signed-rank test; Fig. 6C). Most importantly, when we examined the correlations between human participant ERP waveforms, we found that the majority of the ERP waveforms were significantly correlated (at $p < 0.0013$; Proportion of comparisons with significant correlations: dACC: 0.87 ± 0.169; rACC: 0.90 ± 0.115; amygdala: 0.67 ± 0.191), demonstrating an overall similarity across individuals and species in the neural activity induced by a given frequency and current in a given location.

To determine if these high correlations between individuals were reflected in the waveform metrics and PC score maps, we performed two-dimensional cross correlational analyses for rACC and dACC stimulation in the human data set (Fig. 7-B; see Materials and Methods). For both ERP waveform metrics and PC1 score current x frequency maps, two-dimensional cross correlations for rACC stimulation were higher than with dACC stimulation (Fig. 7A–B), indicating that rACC stimulation produced more consistent responses across participants.

Network-level activation depends on frequency, current, and region stimulated with distant activation varying nonlinearly with stimulation frequency

We hypothesized that the nonlinear relationships between frequency and neural response would be reflected in distant, network-level effects of stimulation (Fig. 8A–B). For amplitudes above 4 mA, dACC stimulation induced more widespread voltage changes in absolute AUC (z-scored voltages in the second after

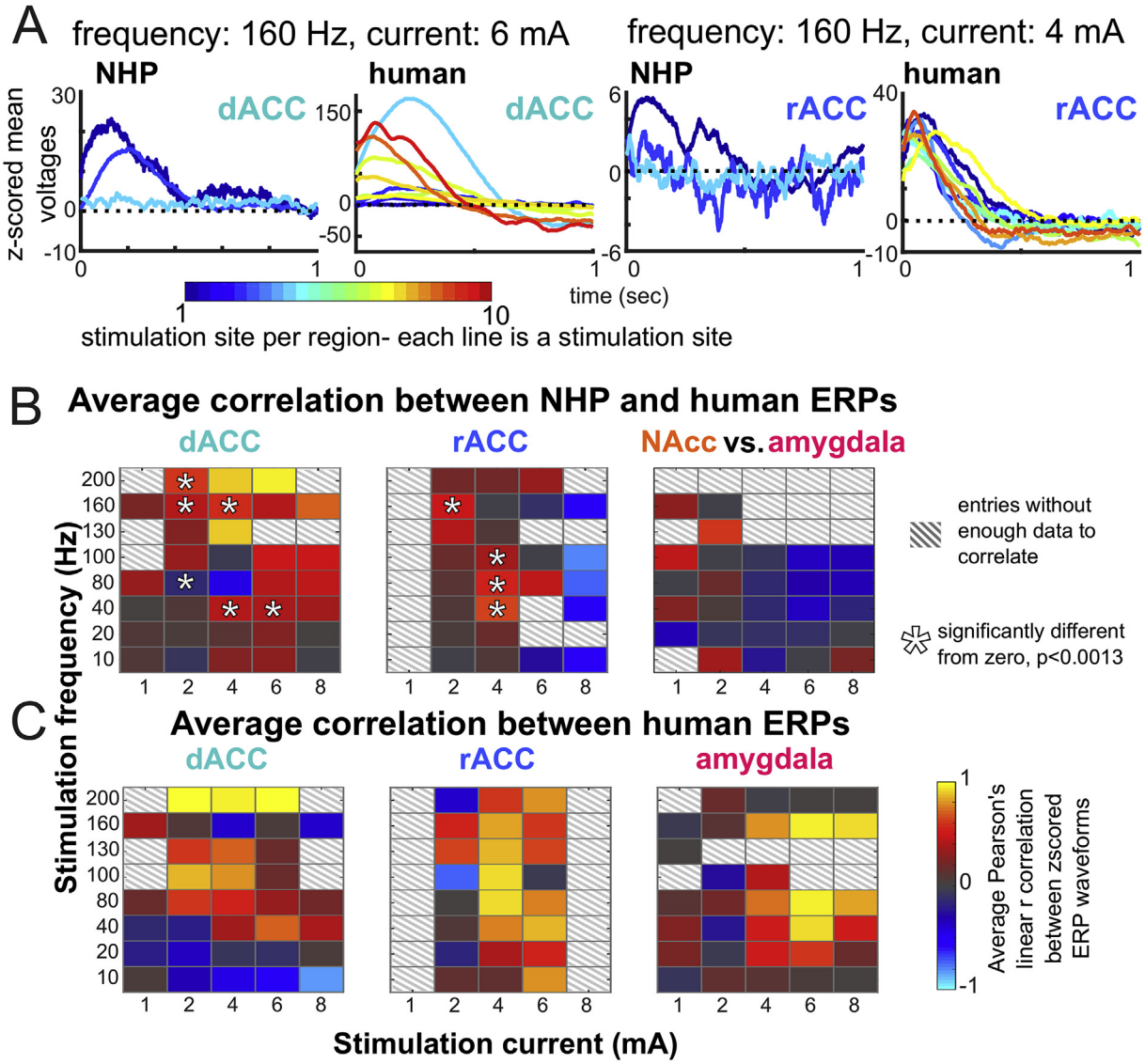

Fig. 6. ERP correlation between individuals and species depends on brain region and frequency. **A**. Z-scored mean local ERP voltage across multiple participants (rainbow color scale) in the dACC (top) and rACC (bottom). **B**. Average correlation values between human and non-human primate ERP z-scored waveforms. White *: significantly different from zero, $p < 0.0013$, Wilcoxon rank sum test. **C**. Average correlation values between only the human z-scored ERP waveforms. (For interpretation of the references to color in this figure legend, the reader is referred to the Web version of this article.)

stimulation) than other stimulation sites, in both species and irrespective of frequency (Fig. 8A–C). Yet, when subdivided by brain region, changes in voltage were similar across stimulation sites, particularly at higher frequencies (Fig. 8C–D; Supplementary Fig. 9).

In another measure of network activation, after mapping the spread of PC waveforms to a standard brain, we found larger PC1 and PC2 scores locally around each region stimulated (Supplementary Fig. 8). Calculating Euclidean distances between stimulation sites and recording sites with absolute PC scores 2 standard deviations above the mean, we found that dACC stimulation induced high PC score spread which varied nonlinearly with frequency. In contrast, rACC stimulation had a significant negative correlation between frequency and spread (PC1: rho = −0.2753; p = 3.73e-06; PC2: rho = −0.1786; p = 0.0042; Supplementary Fig. 8). Thus, with aid of the PCA projection we observe that the relationship between input frequency and the degree to which distal areas are recruited is dependent on stimulation location.

PCA can be used to predict responses across participants

Unlike ERP metrics, PCA can be used to reconstruct entire ERP waveforms by linearly combining PC scores and coefficients. We thus tested whether ERPs could be predicted by modeling the PC scores' dependence on stimulation parameters. We used a model fit to the entire dataset to determine the functional relationship between the first 3 PCs and the stimulation frequency and current. The best-fitting models assumed linear relationships between PC1 scores and frequency and current. PC2 scores had a quadratic relationship with stimulation parameters in both the dACC and rACC. In the amygdala, all 3 PC scores were linearly related to both stimulation frequency and current (Table A 5). Next, to test prediction across individuals, we predicted each participant's z-scored ERPs with a linear model trained on the remaining data (N = 10 for dACC; N = 8 for rACC; Fig. 9A–B; Supplementary Fig. 10). Predicted voltages for dACC and rACC stimulation were highly correlated with the test responses at and above 4 mA (Fig. 9C; Supplementary

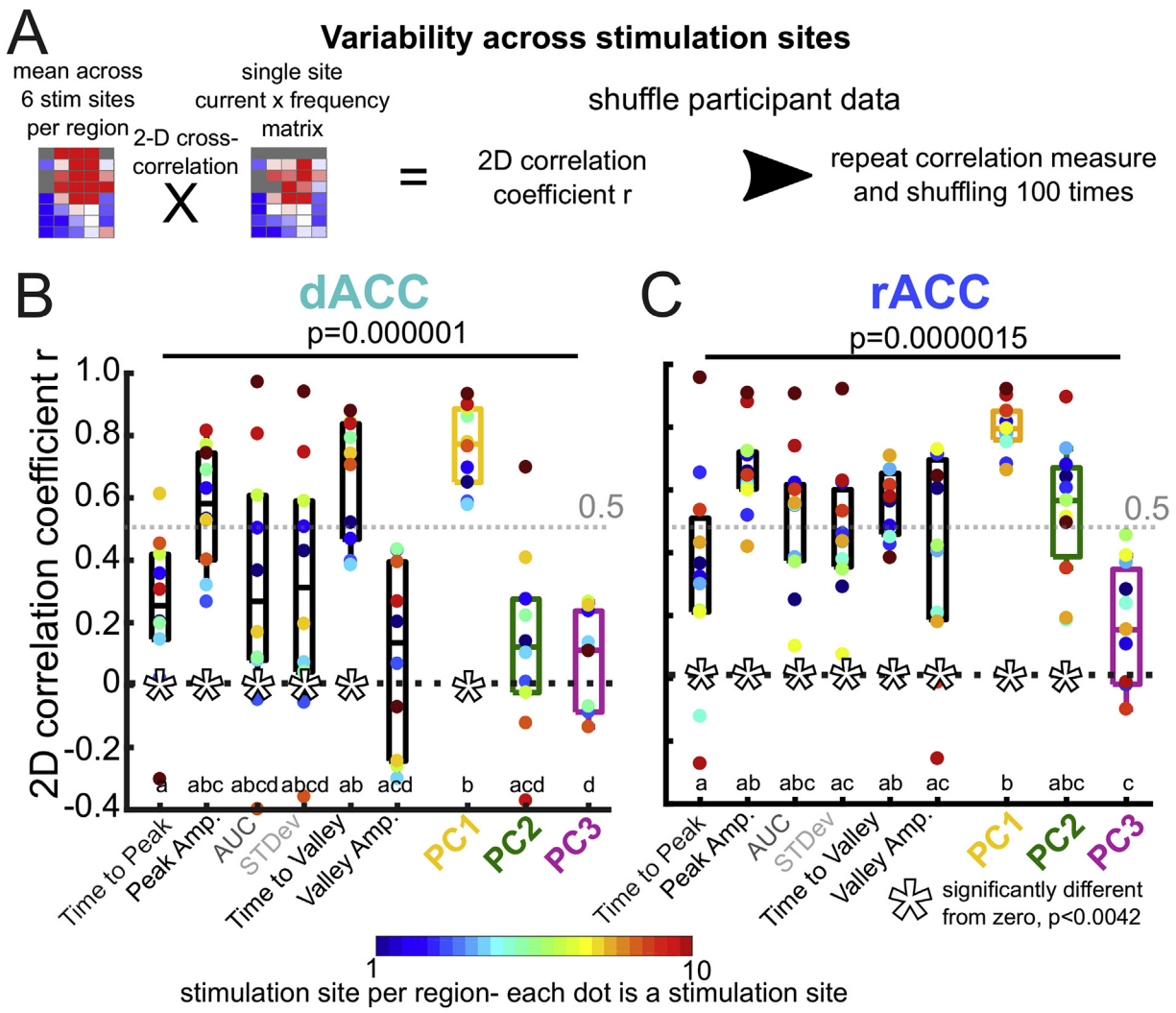

Fig. 7. ERP consistency depends on brain region and frequency. **A.** Method to estimate variability through 2D cross-correlation. **B**. Mean correlation values r between current x frequency maps across individual for dACC stimulation for six ERP metrics and for PC1-PC3 scores with the local responses. **C**. Mean correlation values r between current x frequency maps across individual for the rACC for six ERP metrics and for PC1-PC3 scores with the local responses. **B**–**C**. The colormap in **C** indicates stimulation sites and maps to the different color lines and the different scatterplot dots. p-values indicate significant differences; Kruskal-Wallis test. a-d letters indicate significantly separable groups, identified with a *post hoc* Tukey-Kramer test. (For interpretation of the references to color in this figure legend, the reader is referred to the Web version of this article.)

Fig. 10). We did not have enough samples to test the same linear fit for the amygdala or for the NHP data.

PCA can be used to predict responses to interleaved frequencies

We next examined whether we could leave out half of the stimulation frequencies (10, 40, 100, 160 Hz), build the linear model, and predict the interleaved 'missing' responses. The purpose of this approach was not to perform a cross-validation approach but, instead, was to demonstrate that we could sample neural responses to a subset of frequencies while accurately predicting responses to others. In other words, this approach would allow us to perform tests that are less granular than presented here in other brain regions. We found we could predict higher frequency responses, particularly at high current values (Fig. 10A–B; Supplementary Fig. 11), but prediction accuracy was decreased at lower frequencies and currents (Fig. 10C). Overall, these results confirm that input-output relationships are consistent across individuals and frequencies in PC space as such consistency is necessary for model-based predictions.

Discussion

While direct electrical neural stimulation is a key therapeutic tool for many diseases, we have limited knowledge about the neural response to different stimulation parameters [8,10]. Thus, we explored ERPs across a range of frequencies and currents for short trains of stimulation. We applied these stimuli in multiple brain regions and in both human and non-human primates. Cortical responses depended linearly on the input current, but non-linearly on frequency. As could be expected, there was a clear threshold effect with current in that only certain current levels induced responses. Interestingly, however, the two-way ANOVA results could indicate that the effects of frequency and current on the ERP are independent and therefore likely working through different mechanisms. For instance, frequency changes strongly affected ERP peak timing, particularly in the cingulate. The neural response was not simply correlated with injected energy (the CxF measure); specific frequencies induced maximal amplitude response while also reducing the time to peak. These frequency response differences between brain regions could be key in developing targeted

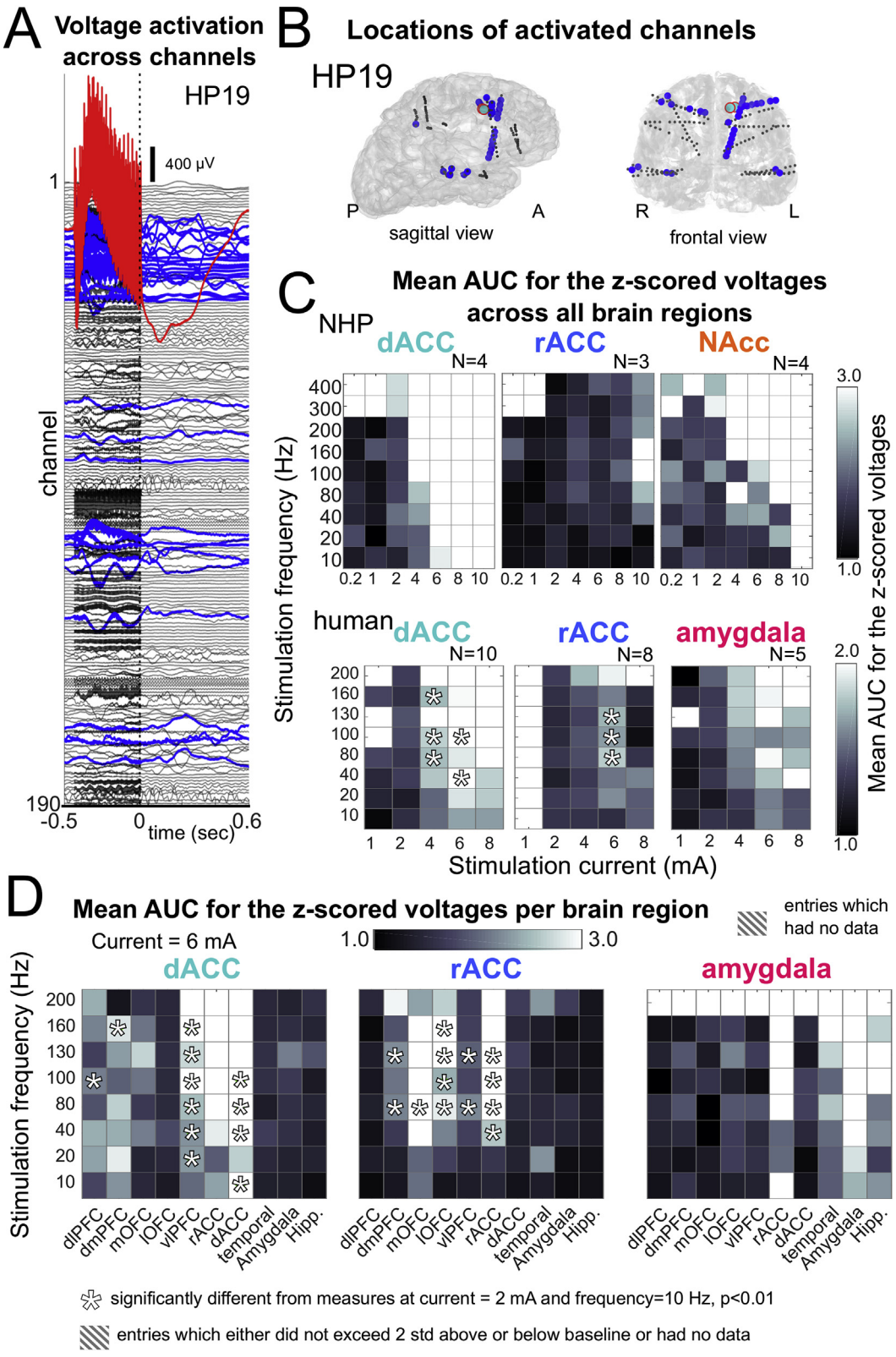

Fig. 8. Network engagement map. **A.** Responses across brain channels (global responses) in one individual, HP19. Blue traces show responses that reach activation threshold (5 STD above or below the mean for >100 ms), while grey traces did not pass threshold. The red trace is an electrode near to the site of stimulation. **B.** Locations in the brain with supra-threshold ERP responses for HP19. **C.** Mean absolute area under the curve (AUC) for the z-scored ERPs across the brain averaged across NHPs (top) and human participants (bottom) with different stimulation targets. **D.** Mean absolute AUC for the z-scored ERPs, averaged across all human recordings, broken down by brain regions, at current = 6 mA. **C, D.** White *-p<0.001, significantly different from current = 2 mA, 10 Hz, Wilcoxon rank sum test. (For interpretation of the references to color in this figure legend, the reader is referred to the Web version of this article.)

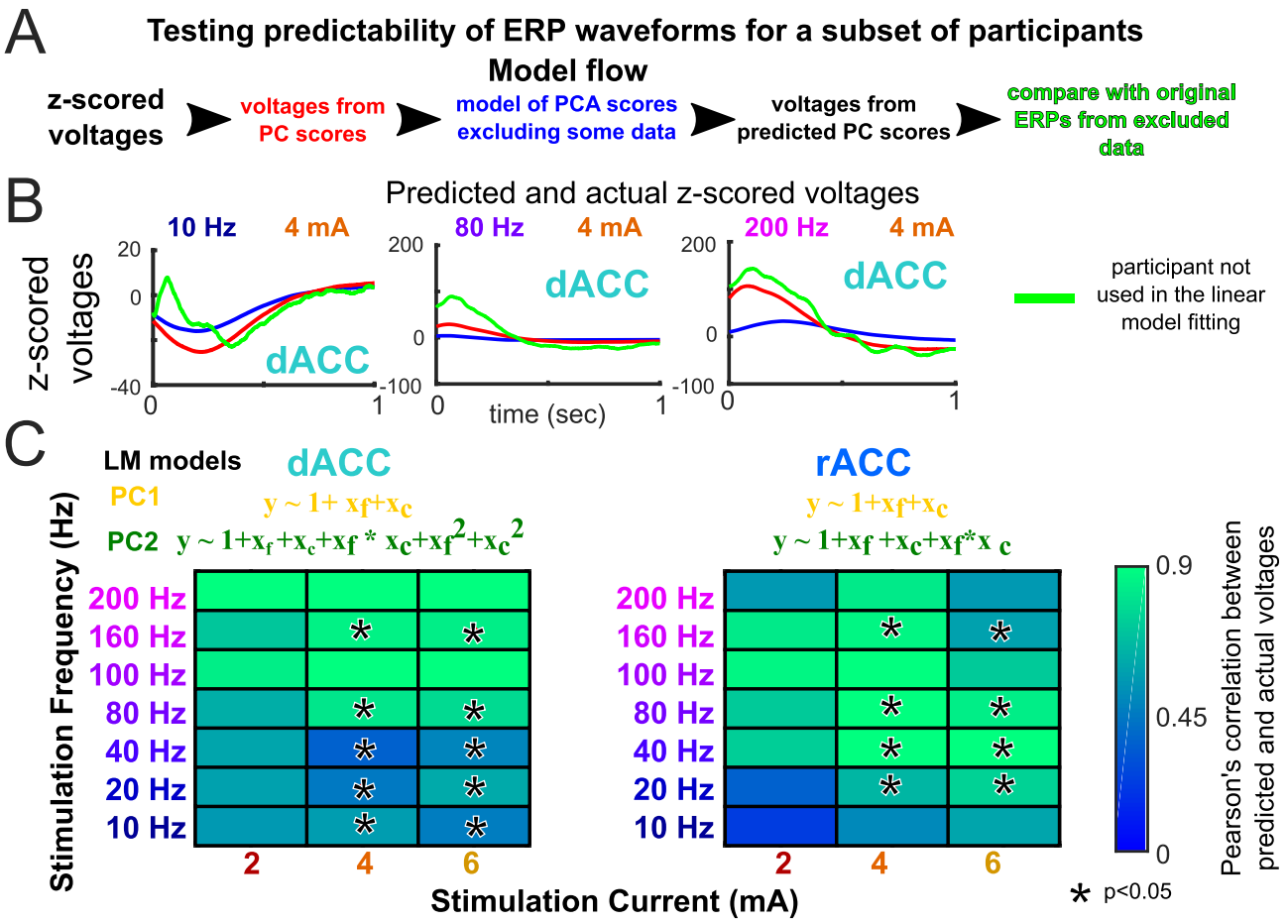

Fig. 9. Local ERP waveforms can be predicted using linear models for individual participants by mapping the PC relationship between frequency and current. **A.** Method to determine the relationship between PC scores for PC1-PC2 (red) to currents and frequencies to then predict z-scored voltages using all participants (black) versus a subset of participants (blue). **B.** Actual and predicted mean z-scored local ERP values, with voltages determined by the original PC1-PC2 scores (red line), the predicted PC scores based on the linear models (in **C**) determined from all but one participant (blue line), and the z-scored voltages for HP19 (green lines). **C.** Pearson's correlation coefficient between actual z-scored voltages for each instance of individual participants left out of the linear model fitting and those predicted by the PC scores multiplied by the relevant PC coefficients to recreate the voltages from the linear model determined by the subset of participants (blue lines in **B**). *- $p < 0.05$ correlation values significantly different from zero, Wilcoxon signed rank test. (For interpretation of the references to color in this figure legend, the reader is referred to the Web version of this article.)

region-specific therapies [4,5,56,57]. Finally, we found that decomposing the ERP waveforms using PCA enabled us to better describe and predict the ERPs in the current-frequency map.

Of course, a major question is how this type of stimulation could be changing activity at the level of single cells or local circuits. Indeed, there is evidence that the local GABAergic and excitatory neural populations respond to stimulation differentially depending on frequency, more specifically in the subthalamic nucleus [27,28]. As might be expected, researchers have found some degree of neural plasticity in this region depends on the frequency of the stimulation [27,28]. Future work might include single cell recordings in the cingulate cortex, amygdala, and nucleus accumbens to better understand the population-level effects we are reporting and to enable more biophysically-relevant models of the neural response profiles. Alternatively, this biophysical modeling might be conducted at the mean-field level, and might be a useful complementary approach to building an atlas of brain stimulation. We recently showed that a relatively simple mean-field model can generate responses very similar to brain stimulation ERPs, and that model predictions track stimulation responses across multiple days [58].

Although we were able to collect a substantial dataset comprising responses to stimulation in cortical and subcortical regions of the human and NHP brain, we did not sweep through a wider parameter range such as stimulation train duration, pulse width and electrode configuration. After-effects of high frequency stimulation can last seconds to minutes, e.g. the brief delay between offset of anti-tremor DBS and the return of full-intensity motor symptoms. We attempted to mitigate these effects by randomly interlacing the low and high frequency stimulation trials. Relevant to this, we also did not test the long-term stimulation effects such as how ERPs could change after a few hours or a day from one stimulation session. This could also affect how the brain responds to stimulation. Although we used an epilepsy cohort as our human subject population, we stimulated in regions that were not identified as epileptogenic. However, this does not preclude the possibility of the responses being different in other subject populations. The NHP subjects, on the other hand, were free from any detectable neurologic condition. We found significant correlations between the neural responses in the NHPs and the human participants. Since we observed similar responses across these species particularly in the dACC, we believe that the response profiles we report are likely to be present in healthy brain tissue.

The stimulation site was a key determinant of ERP current-frequency maps, whether using voltage metrics or PCA. For instance, ERPs were different even between two cingulate regions,

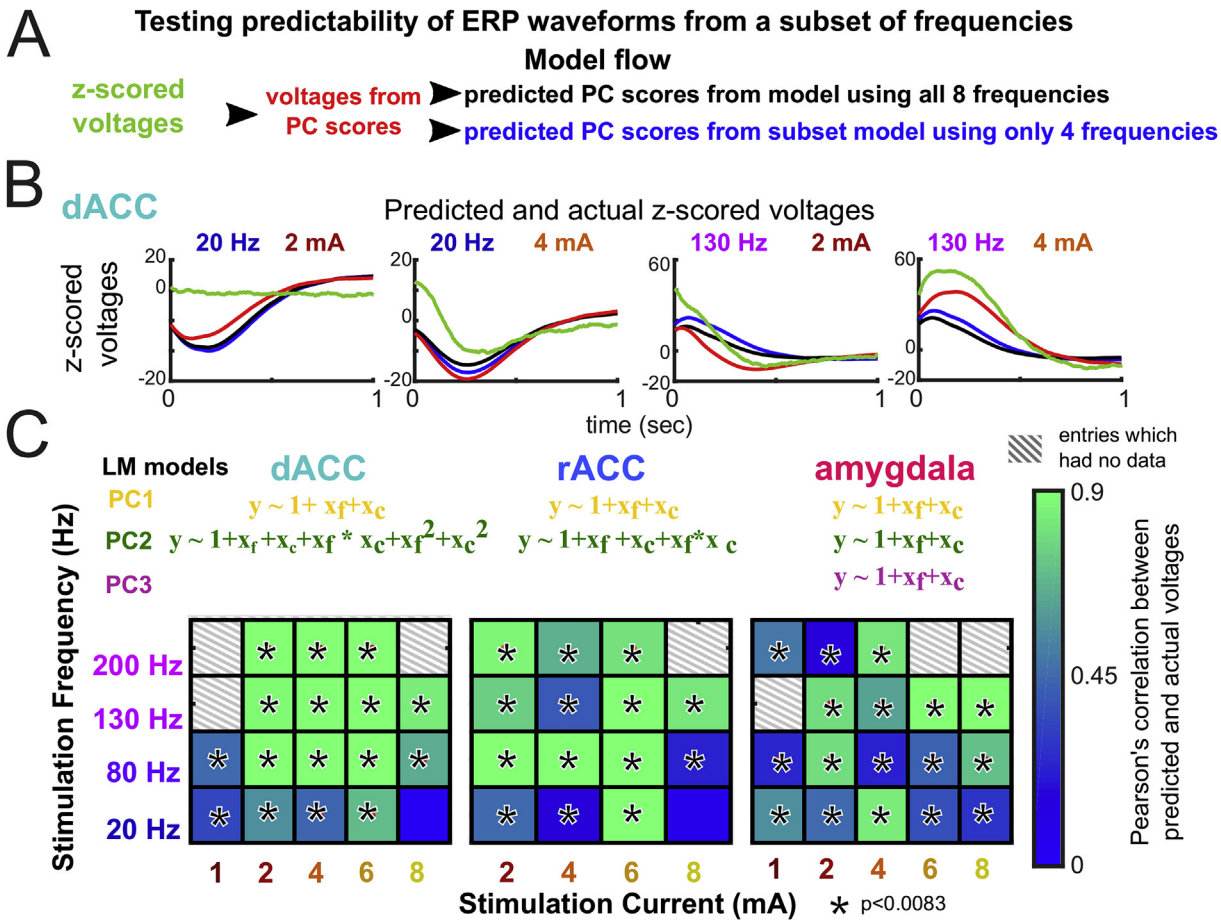

Fig. 10. Local ERP waveforms can be predicted using linear models for specific frequencies by mapping the PC relationship between frequency and current. **A.** Method to determine the relationship between PC scores for PC1-PC2 (red) to currents and frequencies to then predict z-scored voltages using all frequencies (black) or a subset of frequencies (blue). **B.** Voltages predicted PC scores for PC1-PC3 (red) to currents and frequencies to then predict z-scored voltages using a subset of frequencies (blue) versus all frequencies (black). Actual and predicted mean z-scored ERP values, with voltages determined by the original PC1-PC3 scores (red line), the predicted PC scores based on the linear models (in **C**) determined from the entire range of frequencies (black line; 10, 20, 40, 80, 100, 130, 160, 200 Hz) and from a subset of frequencies (blue line; 10, 40, 100, 160 Hz), and the z-scored voltages (green line). **C.** Linear models of the PC scores, indicated by the yellow (PC1), green (PC2), and maroon (PC3) equations, were used to predict the responses to a subset of frequencies (20, 80, 130, 200 Hz) at different current amplitudes. * - indicate significant Pearson correlation coefficients, $p < 0.0083$. (For interpretation of the references to color in this figure legend, the reader is referred to the Web version of this article.)

the rACC and dACC, despite high correlation values between individual responses. Additionally, the input-output relationship with frequency differed between locations. For example, the cingulate targets demonstrated nonlinear frequency-output relationships, while the amygdalar stimulation responses scaled linearly with both frequency and current. Stimulation location also altered the spread of ERPs to other brain regions, with more spread from dACC stimulation versus other brain region targets globally.

These results are consonant with therapeutic observations that efficacy depends on the precise contact stimulated [59], which suggests there are small regional differences in the neurophysiological effects of stimulation. Nonetheless, in this study in which positioning was not intended to be exactly homologous across patients, we still observed significant correlation in the relationship between position of the stimulating electrode and input-output functions across species and individuals. In fact, it is possible that the variability we did observe was, in part, due to those small differences in positioning, and therefore subregion activation. Overall this suggests that large scale input-out relationships are regional but that millimeter scale anatomical precision may subtly alter exact response characteristics.

To better describe and predict the ERP waveform based on these input-output relationships, we used PCA decomposition. We demonstrated a brain region-specific algorithm to predict ERPs using the first 2–3 PCs and scores. Using PCA, we established the relationship between the PC scores and stimulation frequency; PC1 varied with the amount of injected energy (CxF) across brain regions, PC2 varied with current and frequency in more complex relationships in the cingulate (with interaction and quadratic terms) but varied linearly in the amygdala, while PC3 varied linearly with current and frequency with amygdala stimulation (and actually played a minor role for stimulation elsewhere). These results revealed relationships between current, frequency, and stimulated brain region that were specific to the brain region being examined that were not possible through other ERP measures such as peak amplitude.

The use of PCA allowed us to predict voltage responses across individuals and frequencies. This suggests the concept of an atlas of stimulation responses, which could be used as a basis for designing experiments and therapeutic interventions. Moving forward, we suggest that this strategy be used to expand the cartography of "known stimulus space" in a principled fashion on a per-brain region level. If our PCA and model approach holds true in other brain regions, expansive and detailed coverage of the entire stimulation space would no longer be necessary. Instead, a relatively limited set of discrete current x frequency points could be obtained for a

specific brain area and a PC based model should predict the remainder of responses. Interestingly, we could not use a linear interpolation of the responses between frequencies to predict responses for the 'missing' frequencies since 1) the responses, particularly in the cingulate, demonstrated a non-linear relationship to frequency and 2) in our model fit, we find that PC2, in particular, required quadratic and interaction terms to best describe the data and then predict the response in the cingulate targets, further indicating that the response is not simply directly proportional to the frequency of stimulation. This could mean that a similar approach taking into account some of the nonlinear dynamics with the use of PC might hold for other stimulation parameters such as phase, pulse width, and train duration, though this result remains to be tested. To accelerate the development of such an atlas, the data from this study is available in a public repository (https://transformdbs.partners.org/) where other researchers in the community can add stimulation data from other brain regions to extend the mapping. This atlas could help design rational therapies based on both the local and network responses to brain stimulation [9].

Conclusions

We characterized multiple brain regions' stimulation response profiles and found a nonlinear, distance- and region-dependent relationship to stimulation frequency that was consistent across species and individuals. This consistency permitted mapping of response waveforms based on principal components, a foundational step in creating predictive maps to guide brain stimulation.

Declaration of conflicts of interest

The authors declare no competing financial interests and there are no personal relationships with other people or organizations that could have inappropriately influenced the work.

Prior presentation of the research

"The nonlinear relationship between stimulation frequency, amplitude and local responses in cortical and subcortical regions of the human and non-human primate brain", *M. M. Robertson, I. Basu, A. C. Paulk, K. Farnes, D. I. Vallejo, B. Crocker, D. D. Dougherty, E. N. Eskandar, A. S. Widge, S. S. Cash; (poster) Society for Neuroscience 47th Annual Meeting, Washington, DC, U. S. A. Nov. 11 - 15.

Acknowledgments

We would like to thank Giovanni Piantoni, Jean-Baptiste Eichenlaub, Erica Johnson, Gavin Belok, Mia Borzello, and Pariya Salami for help in data collection.

Appendix A. Supplementary data

Supplementary data to this article can be found online at https://doi.org/10.1016/j.brs.2019.03.007.

Funding

Support included NIH grants MH086400, DA026297, and EY017658 to ENE, MH109722, NS100548, and MH111872 to ASW, NS100548 to DDD, and ECOR and K24-NS088568 to SSC. This research was also supported in part by the U.S. Army Research Office and Defense Advanced Research Projects Agency under Cooperative Agreement Number W911NF-14-2-0045 issued by ARO contracting office in support of DARPA's SUBNETS Program. The views, opinions, and/or findings expressed are those of the authors and should not be interpreted as representing the official views or policies of the National Institutes of Health, Department of Defense, or the U.S. Government.

References

[1] Lozano AM, Lipsman N. Probing and regulating dysfunctional circuits using deep brain stimulation. Neuron 2013;77:406–24. https://doi.org/10.1016/j.neuron.2013.01.020.
[2] Widge AS, Dougherty DD. Deep brain stimulation for treatment-refractory mood and obsessive-compulsive disorders. Curr Behav Neurosci Rep 2015;2:187–97. https://doi.org/10.1007/s40473-015-0049-y.
[3] Bronstein JM, Tagliati M, Alterman RL, Lozano AM, Volkmann J, Stefani A, et al. Deep brain stimulation for Parkinson disease: an expert consensus and review of key issues. Arch Neurol 2011;68:165–71. https://doi.org/10.1001/archneurol.2010.260.
[4] Mayberg HS, Lozano AM, Voon V, McNeely HE, Seminowicz D, Hamani C, et al. Deep brain stimulation for treatment-resistant depression. Neuron 2005;45:651–60. https://doi.org/10.1016/j.neuron.2005.02.014.
[5] Perlmutter JS, Mink JW. Deep brain stimulation. Annu Rev Neurosci 2006;29:229–57. https://doi.org/10.1146/annurev.neuro.29.051605.112824.
[6] Widge AS, Malone DA, Dougherty DD. Closing the loop on deep brain stimulation for treatment-resistant depression. Front Neurosci 2018;12:175. https://doi.org/10.3389/fnins.2018.00175.
[7] Bourne SK, Eckhardt CA, Sheth SA. Mechanisms of deep brain stimulation for obsessive compulsive disorder: effects upon cells and circuits. Front Integr Neurosci 2012;6:29. https://doi.org/10.3389/fnint.2012.00029.
[8] Chiken S, Nambu A. Mechanism of deep brain stimulation: inhibition, excitation, or disruption? Neuroscientist 2015;22:313–22. https://doi.org/10.1177/1073858415581986.
[9] Mcintyre CC, Hahn PJ. Network perspectives on the mechanisms of deep brain stimulation. Neurobiol Dis 2010;38:329–37. https://doi.org/10.1016/j.nbd.2009.09.022.
[10] Herrington TM, Cheng JJ, Eskandar EN. Mechanisms of deep brain stimulation. J Neurophysiol 2016;115:19–38. https://doi.org/10.1152/jn.00281.2015.
[11] Boëx C, Vulliémoz S, Spinelli L, Pollo C, Seeck M. High and low frequency electrical stimulation in non-lesional temporal lobe epilepsy. Seizure 2007;16:664–9. https://doi.org/10.1016/j.seizure.2007.05.009.
[12] Brocker DT, Grill WM. Principles of electrical stimulation of neural tissue. first ed., vol. 116. Elsevier B.V.; 2013. https://doi.org/10.1016/B978-0-444-53497-2.00001-2.
[13] Meador KJ, Kapur R, Loring DW, Kanner AM, Morrell MJ. Quality of life and mood in patients with medically intractable epilepsy treated with targeted responsive neurostimulation. Epilepsy Behav 2015;45:242–7. https://doi.org/10.1016/j.yebeh.2015.01.012.
[14] Mcintyre CC, Foutz TJ. Computational modeling of deep brain stimulation. Handb Clin Neurol 2013;116:55–61. https://doi.org/10.5588/ijtld.16.0716.Isoniazid.
[15] Seo H, Jun SC. Multi-scale computational models for electrical brain stimulation. Front Hum Neurosci 2017;11:1–14. https://doi.org/10.3389/fnhum.2017.00515.
[16] Cogan SF, Ludwig KA, Welle CG, Takmakov P, Clinic M, Spring S, et al. Tissue damage thresholds during therapeutic electrical stimulation. J Neural Eng 2016;13:021001. https://doi.org/10.1088/1741-2560/13/2/021001 [Tissue].
[17] Krames ES, Peckham PH, Rezai AR, editors. Neuromodulation. second ed. Academic Press; 2018.
[18] Goetz SM, Deng Z. The development and modeling of devices and paradigms for transcranial magnetic stimulationvol. 29; 2017. p. 115–45.
[19] Huang Y, Liu AA, Lafon B, Friedman D, Dayan M, Wang X, et al. Measurements and models of electric fields in the in vivo human brain during transcranial electric stimulation. elife 2017;6:1–26.
[20] Miranda PC, Callejón-Leblic MA, Salvador R, Ruffini G. Realistic modeling of transcranial current stimulation: the electric field in the brain. Curr Opin Biomed Eng 2018;8:20–7. https://doi.org/10.1016/j.cobme.2018.09.002.
[21] Opitz A, Yeagle E, Thielscher A, Schroeder C, Mehta AD, Milham MP. On the importance of precise electrode placement for targeted transcranial electric stimulation. Neuroimage 2018;181:560–7. https://doi.org/10.1016/j.neuroimage.2018.07.027.
[22] Opitz A, Falchier A, Yan CG, Yeagle EM, Linn GS, Megevand P, et al. Spatiotemporal structure of intracranial electric fields induced by transcranial electric stimulation in humans and nonhuman primates. Sci Rep 2016;6:1–11. https://doi.org/10.1038/srep31236.
[23] Valero-Cabré A, Amengual JL, Stengel C, Pascual-Leone A, Coubard OA. Transcranial magnetic stimulation in basic and clinical neuroscience: a comprehensive review of fundamental principles and novel insights [Internet]. Neurosci Biobehav Rev 2017;83:381–404. https://doi.org/10.1016/j.neubiorev.2017.10.006.
[24] Chkhenkeli SA, Šramka M, Lortkipanidze GS, Rakviashvili TN, Bregvadze ES, Magalashvili GE, et al. Electrophysiological effects and clinical results of direct brain stimulation for intractable epilepsy. Clin Neurol Neurosurg 2004;106:318–29. https://doi.org/10.1016/j.clineuro.2004.01.009.

[25] Hamberger MJ, Williams AC, Schevon CA. Extraoperative neurostimulation mapping: results from an international survey of epilepsy surgery programs. Epilepsia 2014;55:933–9. https://doi.org/10.1111/epi.12644.
[26] Donos C, Mîndruță I, Ciurea J, Mălîia MD, Barborica A. A comparative study of the effects of pulse parameters for intracranial direct electrical stimulation in epilepsy. Clin Neurophysiol 2016;127:91–101. https://doi.org/10.1016/j.clinph.2015.02.013.
[27] Milosevic L, Kalia SK, Hodaie M, Lozano AM, Fasano A, Popovic MR, et al. Neuronal inhibition and synaptic plasticity of basal ganglia neurons in Parkinson's disease. Brain 2018;141:177–90. https://doi.org/10.1093/brain/awx296.
[28] Milosevic L, Kalia SK, Hodaie M, Lozano AM, Popovic MR, Hutchison WD. Physiological mechanisms of thalamic ventral intermediate nucleus stimulation for tremor suppression. Brain 2018;141:2142–55. https://doi.org/10.1093/brain/awy139.
[29] Bewernick BH, Hurlemann R, Matusch A, Kayser S, Grubert C, Hadrysiewicz B, et al. Nucleus accumbens deep brain stimulation decreases ratings of depression and anxiety in treatment-resistant depression. Biol Psychiatry 2010;67:110–6. https://doi.org/10.1016/j.biopsych.2009.09.013.
[30] Berlim MT, Mcgirr A, Eynde FVD, Fleck MPA, Giacobbe P. Effectiveness and acceptability of deep brain stimulation (DBS) of the subgenual cingulate cortex for treatment-resistant depression : a systematic review and exploratory meta-analysis. J Affect Disord 2014;159:31–8. https://doi.org/10.1016/j.jad.2014.02.016.
[31] Boccard SGJ, Pereira EAC, Moir L, Hartevelt TJV, Kringelbach ML, Fitzgerald JJ, et al. Deep brain stimulation of the anterior cingulate cortex: targeting the affective component of chronic pain. Neuroreport 2014;25:83–8. https://doi.org/10.1097/WNR.0000000000000039.
[32] Sturm V, Lenartz D, Koulousakis A, Treuer H, Herholz K, Klein JC, et al. The nucleus accumbens: a target for deep brain stimulation in obsessive-compulsive- and anxiety-disorders. J Chem Neuroanat 2003;26:293–9. https://doi.org/10.1016/j.jchemneu.2003.09.003.
[33] Langevin JP, Chen JWY, Koek RJ, Sultzer DL, Mandelkern MA, Schwartz HN, et al. Deep brain stimulation of the basolateral amygdala: targeting technique and electrodiagnostic findings. Brain Sci 2016;6:28. https://doi.org/10.3390/brainsci6030028.
[34] Camprodon JA, Rauch SL, Greenberg BD, Dougherty DD, editors. Psychiatric neurotherapeutics: contemporary surgical and device-based treatments. first ed. New York, NY: Humana Press; 2015.
[35] Dougherty DD, Baer L, Cosgrove GR, Cassem EH, Price BH, Nierenberg AA, et al. Prospective long-term follow-up of 44 patients who received cingulotomy for treatment-refractory obsessive-compulsive disorder. Am J Psychiatry 2002;159:269–75. https://doi.org/10.1001/jama.2017.2200.
[36] Luck SJ. An introduction to event-related potentials and their neural origins. Cambridge: MIT Press; 2014. https://doi.org/10.1007/s10409-008-0217-3.
[37] Sur S, Sinha VK. Event-related potential: an overview. Ind Psychiatry J 2009;18:70–3. https://doi.org/10.4103/0972-6748.57865.
[38] Woodman GF. A brief introduction to the use of event-related potentials (ERPs) in studies of perception and attention. Atten Percept Psychophys 2010;72:1–29. https://doi.org/10.3758/APP.72.8.2031.A.
[39] Kent AR, Swan BD, Brocker DT, Turner DA, Gross RE, Grill WM. Measurement of evoked potentials during thalamic deep brain stimulation. Brain Stimulat 2015;8:42–56. https://doi.org/10.1016/j.brs.2014.09.017.
[40] Baker KB, Montgomery EB, Rezai AR, Burgess R, Lüders HO. Subthalamic nucleus deep brain stimulus evoked potentials: physiological and therapeutic implications. Mov Disord 2002;17:969–83. https://doi.org/10.1002/mds.10206.
[41] Devergnas A, Wichmann T. Cortical potentials evoked by deep brain stimulation in the subthalamic area. Front Syst Neurosci 2011;5:1–8. https://doi.org/10.3389/fnsys.2011.00030.
[42] Waters AC, Veerakumar A, Choi KS, Howell B, Tiruvadi V, Bijanki KR, et al. Test–retest reliability of a stimulation-locked evoked response to deep brain stimulation in subcallosal cingulate for treatment resistant depression. Hum Brain Mapp 2018;39:4844–56. Available from: https://doi.org/10.1002/hbm.24327.
[43] Reuter M, Rosas HD, Fischl B. Highly accurate inverse consistent registration: a robust approach. Neuroimage 2010;53:1181–96. https://doi.org/10.1016/j.neuroimage.2010.07.020.
[44] Reuter M, Schmansky NJ, Rosas HD, Fischl B. Within-subject template estimation for unbiased longitudinal image analysis. Neuroimage 2012;61:1402–18. https://doi.org/10.1016/j.neuroimage.2012.02.084.
[45] Dykstra AR, Chan AM, Quinn BT, Zepeda R, Keller CJ, Cormier J, et al. Individualized localization and cortical surface-based registration of intracranial electrodes. Neuroimage 2012;59:3563–70. https://doi.org/10.1016/j.neuroimage.2011.11.046.
[46] Peled N, Gholipour T, Paulk AC, Felsenstein O, Dougherty DD, Widge AS, et al. Invasive electrodes identification and labeling. GitHub Repos 2017. https://doi.org/10.5281/zenodo.1078789. https://github.com/pelednoam/ieil.
[47] Desikan RS, Ségonne F, Fischl B, Quinn BT, Dickerson BC, Blacker D, et al. An automated labeling system for subdividing the human cerebral cortex on MRI scans into gyral based regions of interest. Neuroimage 2006;31:968–80. https://doi.org/10.1016/j.neuroimage.2006.01.021.
[48] Holmes CJ, Hoge R, Collins L, Woods R, Toga AW, Evans AC. Enhancement of MR images using registration for signal averaging. J Comput Assist Tomogr 1998;22:324–33.
[49] Postelnicu G, Zöllei L, Fischl B. Combined volumetric and surface registration. October 2009;28:508–22. https://doi.org/10.1109/TMI.2008.2004426.
[50] Bakker R, Tiesinga P, Kötter R. The Scalable Brain Atlas: instant web-based access to brain atlases and related content. Neuroinformatics 2015;13:353–66. https://doi.org/10.1007/s12021-014-9258-x.
[51] Calabrese E, Badea A, Coe CL, Lubach GR, Shi Y, Styner MA, et al. A diffusion tensor MRI atlas of the postmortem rhesus macaque brain. Neuroimage 2015;117:408–16. https://doi.org/10.1016/j.neuroimage.2015.05.072.A.
[52] Paxinos G, Huang XF, Toga AW. The rhesus monkey brain in stereotaxic coordinates. Academic Press; 2000.
[53] Dubach MF, Bowden DM. BrainInfo online 3D macaque brain atlas: a database in the shape of a brain. Soc Neurosci Annu Meet Chic IL 2009. Abstract No. 199.5.
[54] Rohlfing T, Kroenke CD, Sullivan EV, Dubach MF, Bowden DM, Grant KA, et al. The INIA19 template and NeuroMaps atlas for primate brain image parcellation and spatial normalization. Front Neuroinf 2012;6:1–15. https://doi.org/10.3389/fninf.2012.00027.
[55] Bromm B, Scharein E. Principal component analysis of pain-related cerebral potentials to mechanical and electrical stimulation in man. Electroencephalogr Clin Neurophysiol 1982;53:94–103. https://doi.org/10.1016/0013-4694(82)90109-2.
[56] Bilge MT, Gosai A, Widge AS. Deep brain stimulation in psychiatry: mechanisms, models, and next-generation therapies. Psychiatr Clin North Am 2018;11:373–83.
[57] Widge AS, Ellard KK, Paulk AC, Basu I, Youse A, Zorowitz S, et al. Treating refractory mental illness with closed-loop brain stimulation: progress towards a patient-specific transdiagnostic approach. Exp Neurol 2017;287:461–72. https://doi.org/10.1016/j.expneurol.2016.07.021.
[58] Basu I, Crocker B, Farnes K, Robertson MM, Paulk AC, Vallejo DI, et al. A neural mass model to predict electrical stimulation evoked responses in human and non-human primate brain. J Neural Eng 2018;15:066012.
[59] Fox MD, Buckner RL, Liu H, Chakravarty MM, Lozano AM, Pascual-Leone A. Resting- state networks link invasive and noninvasive brain stimulation across diverse psychiatric and neurological diseases. Proc Natl Acad Sci Unit States Am 2014;111(41):E4367–75.